Inorg. Chem. **2004**, *43*, 7605–7616

Mixed Valence Mn(II)/Mn(III) [3 × 3] Grid Complexes: Structural, Electrochemical, Spectroscopic, and Magnetic Properties

Laurence K. Thompson,* Timothy L. Kelly, Louise N. Dawe, Hilde Grove, and Martin T. Lemaire

Department of Chemistry, Memorial University, St. John's, Newfoundland, A1B 3X7 Canada

Judith A. K. Howard and Elinor C. Spencer

Department of Chemistry, University of Durham, South Road, Durham, DH1 3LE U.K.

Craig J. Matthews and Stuart T. Onions

Division of Chemistry, School of Science, Nottingham Trent University, Clifton Lane, Nottingham, NG11 8NS U.K.

Simon J. Coles, Peter N. Horton, Michael B. Hursthouse, and Mark E. Light

EPSRC National Crystallographic Service, Department of Chemistry, University of Southampton, Highfield, Southampton, SO17 1BJ U.K.

Received June 17, 2004

$Mn(II)_9$ grid complexes with a $[Mn_9(\mu\text{-}O)_{12}]$ core, obtained by self-assembly of a series of tritopic picolinic dihydrazone ligands with Mn(II) salts, have been oxidized by both chemical and electrochemical methods to produce mixed oxidation state systems. Examples involving $[Mn(III)_3Mn(II)_6]$ and $[Mn(III)_4Mn(II)_5]$ combinations have been produced. Structures are reported for $[Mn_9(2poap\text{-}2H)_6](NO_3)_6\cdot 14H_2O$ (**1**), $[Mn_9(2poap\text{-}2H)_6](ClO_4)_{10}\cdot 10H_2O$ (**3**), and $[Mn_9(Cl2poap\text{-}2H)_6](ClO_4)_9\cdot 14H_2O\cdot 3CH_3CN$ (**10**). Structural studies show distinct contraction of the corner grid sites on oxidation, with overall magnetic properties consistent with the resulting changes in electron distribution. Antiferromagnetic exchange in the outer ring of eight metal centers creates a ferrimagnetic subunit, which undergoes antiferromagnetic coupling to the central metal, leading to $S = {}^1/_2$ (**3**) and $S = {}^2/_2$ (**10**) ground states. Two moderately intense absorptions are observed on oxidation of the Mn(II) grids in the visible and near-infrared (1000 nm, 700 nm), associated with charge transfer transitions (LMCT, IVCT respectively). Compound **1** crystallized in the monoclinic system, space group $P2_1/n$, with $a = 21.308(2)$ Å, $b = 23.611(2)$ Å, $c = 32.178(3)$ Å, $\beta = 93.820(2)°$. Compound **3** crystallized in the tetragonal system, space group $I\bar{4}$, with $a = b = 18.44410(10)$ Å, $c = 24.9935(3)$ Å. Compound **10** crystallized in the triclinic system, space group $P\bar{1}$, with $a = 19.1150(10)$ Å, $b = 19.7221(10)$ Å, $c = 26.8334(14)$ Å, $\alpha = 74.7190(10)°$, $\beta = 77.6970(10)°$, $\gamma = 64.7770(10)°$. The facile oxidation of the $Mn(II)_9$ grids is highlighted in terms of their potential use as molecular based platforms for switching and data storage.

Introduction

Preorganized molecular platforms containing closely spaced "flat" [$n \times n$] square arrays of metal ion centers present attractive architectures for surface applications, and two-dimensional "addressing" in the context of device behavior at the molecular level. Examples of [2 × 2], [3 × 3], and [4 × 4] grids involving polypyridine-like "polytopic" ligands are well documented with such metal ions as Co(II), Fe(II) ([2 × 2]),[1−6] Zn(II) ([3 × 3]),[7] and Pb(II) ([4 × 4]),[8] with

* To whom correspondence should be addressed. E-mail: lthomp@mun.ca.

(1) Hanan, G. S.; Volkmer, D.; Schubert, U. S.; Lehn, J.-M.; Baum, G.; Fenske, D. *Angew. Chem., Int. Ed.* **1997**, *36*, 1842.
(2) Waldmann, O.; Hassman, J.; Müller, P.; Hanan, G. S.; Volmer, D.; Schubert, U. S.; Lehn, J.-M. *Phys. Rev. Lett.* **1997**, *78*, 3390.
(3) Ruben, M.; Breuning, E.; Barboiu, M.; Gisselbrecht, J.-P.; Lehn, J.-M. *Chem. Eur. J.* **2003**, *9*, 291.
(4) Ruben, M.; Breuning, E.; Gisselbrecht, J.-P.; Lehn, J. M. *Angew. Chem., Int. Ed.* **2000**, *39*, 4139.

10.1021/ic040083a CCC: $27.50
Published on Web 10/23/2004

Chart 1

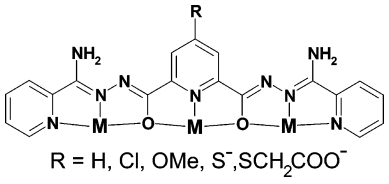

Scheme 1

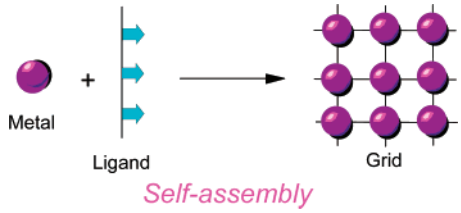

the coordination pockets connected by pyrimidine bridging subunits. Electrochemical properties of the $Co(II)_4$ systems are quite remarkable in that a suite of one-electron reductions is observed with up to 12 electrons accumulating on the hexadentate heterocyclic aromatic ligands.[3,4] Modification of the ligands to include ionizable hydrazone fragments allows access to metal based redox processes.[5]

"Tritopic" ligands based on the 2,6-picolinic acid dihydrazone core (Chart 1) have important coordination information encoded in their organic molecular structures, such that they self-assemble in the presence of metal ions to produce [3 × 3] nonanuclear grid complexes in high yields (Scheme 1), with examples involving Mn(II), Fe(III), Cu(II), and Zn(II) ions.[9−17] The Mn(II) complexes exhibit well defined electrochemical and magnetic properties, and solution studies indicate that groups of metal ions within the grid can be selectively oxidized from Mn(II) to Mn(III). This results in a corresponding change in overall magnetic properties consistent with the reduced electron complement within the grid, associated with the mixtures of high spin Mn(II) and Mn(III) sites.[9,17] The isolation of a $[Mn(II)_6Mn(III)_3]$ grid complex in crystalline form, and subsequent crystallographic analysis, has shown that the corner Mn(II) centers are the first to oxidize as a group within the potential range 0.5−1.0 V (vs SSCE), and that the oxidation sequences can be affected by both chemical and electrochemical means.[17]

In the present study, we describe other oxidized grid species, within the general class $[Mn(II)_{9-x}Mn(III)_x]$ (x = 1−4), which have been produced both chemically and electrochemically. Cyclic voltammetry and differential pulse voltammetry studies are described, with an assessment of the degree of oxidation based on electrochemical, magnetic, and spectroscopic data. As oxidation proceeds, the color of acetonitrile solutions of the Mn(II) grids changes from orange to dark brown, with the appearance intense charge transfer absorptions in the visible and near-infrared regions, associated with both Mn(II) to Mn(III) metal-to-metal charge transfer and ligand to Mn(III) charge transfer processes. The grids are discussed as multistable molecular platforms for switching and data storage and are considered as potential molecular components in a "bottom up" approach to molecular based electronic devices.

Experimental Section

Physical Measurements. Infrared spectra were recorded as Nujol mulls using a Mattson Polaris FT-IR instrument, and visible and near-infrared absorption spectra with a Cary 5E spectrometer. Microanalyses were carried out by Canadian Microanalytical Service, Delta, Canada. ESR spectra were obtained at room temperature with a Bruker ESP 300 spectrometer. Variable temperature magnetic data (2−300 K) were obtained using a Quantum Design MPMS5S SQUID magnetometer with field strengths in the range 0.01−0.1 T, and magnetization data as a function of field were obtained at 2 K with field strengths in the range 0−5 T. Samples were prepared in gelatin capsules, and mounted inside straws for attachment to the sample transport rod. Background corrections for the sample holder assembly and diamagnetic components of the complexes were applied. Cyclic voltammetry (CV) studies were carried out with a BAS 100B electrochemistry system. A Pt working electrode, Pt counter electrode, and SSCE and saturated Ag/AgCl reference electrodes were used. Solutions were ~1 mM in complex, with added 0.1 M tetraethylammonium perchlorate (TEAP) in acetonitrile. Differential pulse voltammetry was carried out at a 20 mV/s scan rate (50 mV pulse amplitude, 50 ms pulse width) in an oxidative (anodic) sweep. Bulk electrolytic oxidation in acetonitrile/water mixtures was carried out using two electrolytic cell assembles. For cell 1: A Pt mesh anode and a Pt wire cathode contained in a fritted sleeve were connected to a HP6215A DC power supply. $HClO_4$ (70%) was used in the cathode compartment as the sacrificial cathode species. For cell 2: A Pt mesh anode, a Pt mesh cathode in a fritted sleeve, and a saturated Ag/AgCl reference electrode were connected to a HP6215A power supply in conjunction with a high impedance voltmeter (Chemtrix 60A). Current was monitored with a Keithley 172A multimeter. $HClO_4$ (70%) was used as a sacrificial species in the cathode compartment.

Coordination Complexes. $[Mn_9(2poap\text{-}2H)_6](NO_3)_6\cdot 14H_2O$ (1). 2poap[9] (Chart 1, R = H) (0.50 g, 1.24 mmol) was added to a solution of $Mn(NO_3)_2\cdot 6H_2O$ (0.86 g, 3.0 mmol) in MeOH/H_2O (50 mL/50 mL) with stirring and warming. NH_4OH(aq) (20%) was added dropwise with stirring until the pH reached 6.0, with the formation of an orange-brown solution. The volume of the solution was reduced under vacuum until crystals began to form, and the mixture was allowed to stand at room temperature for several days.

(5) Uppadine, L. H.; Gisselbrecht, J.-P.; Lehn, J.-M. *Chem. Commun.* **2004**, 718.
(6) Ruben, M.; Breuning, E.; Lehn, J.-M.; Ksenofontov, V.; Renz, F.; Gütlich, P.; Vaughan, G. B. M. *Chem. Eur. J.* **2003**, *9*, 4422.
(7) Breuning, E.; Hanan, G. S.; Romero-Salguero, F. J.; Garcia, A. M.; Baxter, P. N. W.; Lehn, J.-M.; Wegelius, E.; Rissanen, K.; Nierengarten, H.; van Dorsselaer, A. *Chem. Eur. J.* **2002**, *8*, 3458.
(8) Barboiu, M.; Vaughan, G.; Graff, R.; Lehn, J.-M. *J. Am. Chem. Soc.* **2003**, *125*, 10257.
(9) Zhao, L.; Matthews, C. J.; Thompson, L. K.; Heath, S. L. *J. Chem. Soc., Chem. Commun.* **2000**, 265.
(10) Zhao, L.; Xu, Z.; Thompson, L. K.; Heath, S. L.; Miller, D. O.; Ohba, M. *Angew. Chem., Int. Ed.* **2000**, *39*, 3114.
(11) Waldmann, O.; Koch, R.; Schromm, S.; Müller, P.; Zhao, L.; Thompson, L. K. *Chem. Phys. Lett.* **2000**, *332*, 73.
(12) Waldmann, O.; Zhao, L.; Thompson, L. K. *Phys. Rev. Lett.* **2002**, *88*, 066401.
(13) Zhao, L.; Xu, Z.; Thompson, L. K.; Miller, D. O. *Polyhedron* **2001**, *20*, 1359.
(14) Thompson, L. K.; Zhao, L.; Xu, Z.; Miller, D. O.; Reiff, W. M. *Inorg. Chem.* **2003**, *42*, 128.
(15) Xu, Z.; Thompson, L. K.; Miller, D. O. *Polyhedron* **2002**, *21*, 1715.
(16) Thompson, L. K. *Coord. Chem. Rev.* **2002**, *233*−*234*, 193.
(17) Zhao, L.; Xu, Z.; Grove, H.; Milway, V.; Dawe, L. N.; Abedin, T. S. M.; Thompson, L. K.; Kelly, T. L.; Miller, D. O.; Weeks, L.; Shapter, J. G.; Pope, K. J. *Inorg. Chem.* **2004**, *43*, 3812.

A red-orange crystalline product formed, from which crystals were selected for structural analysis. Yield 0.73 g, 90%. Anal. Calcd for $[Mn_9(C_{19}H_{15}N_9O_2)_6](NO_3)_6 \cdot 14H_2O$ (**1**): C, 38.82; H, 3.37; N, 23.83%. Found: C, 38.82; H, 2.69; N, 23.82%.

$[Mn_9(M2poap)_6](ClO_4)_6 \cdot 22H_2O$ (2). M2poap (Chart 1, R = OMe)[15] (0.43 g, 1.0 mmol) was added to a solution of $Mn(ClO_4)_2 \cdot 6H_2O$ (1.1 g, 3.0 mmol) in $MeOH/CH_3CN/H_2O$ (10 mL/10 mL/3 mL) with warming to form an orange solution. Orange crystals were produced on standing after an extended period (yield 0.66 g, 70%). The crystals were not suitable for X-ray diffraction. Anal. Calcd for $[Mn_9(C_{20}H_{17}N_9O_3)_6](ClO_4)_6 \cdot 22H_2O$ (**2**): C, 35.05; H, 3.67; N, 18.39%. Found: C, 34.87; H, 2.94; N, 18.30%.

Oxidized Complexes Produced by Electrochemical and Chemical Oxidation. $[Mn_9(2poap\text{-}2H)_6](ClO_4)_{10} \cdot 10H_2O$ (3). $[Mn_9(2poap\text{-}2H)_6](ClO_4)_6 \cdot 18H_2O$ (**6**)[9] (480 mg, 0.13 mmol) and tetraethylammonium perchlorate (0.55 g, 2.4 mmol) were dissolved in a mixture of 80 mL of acetonitrile and 50 mL of water, forming a clear orange-red solution. The solution was placed in cell 1 (see Experimental Section), the electrodes were charged to +20 V, to overcome solution resistance, and 5 drops of 70% perchloric acid were added to the cathode compartment. After ca. 4 h, the solution became very dark brown. It was concentrated by evaporation under reduced pressure and chilled in a freezer. A dark brown solid precipitated, which was isolated by suction filtration, washed with diethyl ether, and air-dried. Yield 0.21 g, 39%. Recrystallization from acetonitrile produced dark brown crystals suitable for structural analysis. Anal. Calcd for $[Mn_9(C_{19}H_{15}N_9O_2)_6]\ (ClO_4)_{10} \cdot 10H_2O$ (**3**): C, 33.60; H, 2.72; N, 18.58%. Found: C, 33.55; H, 2.58; N, 18.42%. Selected IR data (Nujol mull, cm^{-1}): 1071 (ν ClO_4^-). ESR spectrum: no signal.

$[Mn_9(Cl2poap\text{-}2H)_6](ClO_4)_9 \cdot 6H_2O$ (4). $[Mn_9(Cl2poap\text{-}2H)_6](ClO_4)_6 \cdot 10H_2O$ (**7**)[14] (Cl2poap; Chart 1, R = Cl) (0.28 g, 0.072 mmol) and tetraethylammonium perchlorate (0.69 g, 3.0 mmol) were dissolved in ~200 mL of a 50/50 acetonitrile/water mixture, forming a clear orange solution. The solution was placed in cell 2 (see Experimental Section), the electrodes were charged to +15 V, and 1 mL of 70% perchloric acid was added to the cathode compartment. The potential was then adjusted to +1.8 V with respect to the saturated Ag/AgCl reference electrode, and maintained at $+1.8 \pm 0.2$ V for ca. 7 h, by which time a brown solution had formed. The solution was concentrated by evaporation under reduced pressure, filtered, and left to stand. After 10 days, large brown crystals formed in solution. The crystals were separated and air-dried. They were not suitable for structural analysis. Yield (0.105 g, 35%). Anal. Calcd for $[Mn_9(C_{19}H_{14}N_9O_2Cl)_6](ClO_4)_9 \cdot 6H_2O$ (**4**): C, 33.34; H, 2.36; N, 18.43%. Found: C, 33.32; H, 2.44; N, 18.38%. Selected IR data (Nujol mull, cm^{-1}): 1094 (ν ClO_4^-).

$[Mn_9(2poap\text{-}2H)_6](NO_3)_{10} \cdot 25H_2O$ (5). $[Mn_9(2poap\text{-}2H)_6](NO_3)_6 \cdot 14H_2O$ (**1**) (0.20 g, 0.056 mmol) and potassium nitrate (2.03 g, 20 mmol) were dissolved in a mixture of 125 mL of acetonitrile and 75 mL of water, forming a clear orange solution (0.1 M in KNO_3). The solution was placed in cell 2, and the electrodes were charged to +1 V versus saturated Ag/AgCl reference electrode. There were 10 drops of 10% nitric acid added to the counter electrode, and the potential was readjusted to $+2.0 \pm 0.1$ V. The electrolysis proceeded for 27 h, at which time no discernible change in current was observed. The very dark brown solution was concentrated by evaporation under reduced pressure and left to stand. After ca. 8 weeks, dark brown lustrous crystals formed. The crystals were not suitable for structural analysis. Yield 0.070 g, 33%. Anal. Calcd for $[Mn_9(C_{19}H_{15}N_9O_2)_6]\ (NO_3)_{10} \cdot 25H_2O$ (**5**): C, 34.46; H, 3.55; N, 22.56%. Found: C, 34.37; H, 3.01; N, 22.54%.

$[Mn_9(Cl2poap\text{-}2H)_6](ClO_4)_6 \cdot 18H_2O$ (9), $[Mn_9(Cl2poap\text{-}2H)_6](ClO_4)_9 \cdot 14H_2O \cdot 3CH_3CN$ (10), $[Mn_9(Cl2poap\text{-}2H)_6](ClO_4)_9 \cdot 14H_2O \cdot 3CH_3CN$ (11). In an attempt to find a chemical method for the synthesis of integer oxidation state Mn(II)/Mn(III) grids, samples of $[Mn_9(Cl2poap\text{-}2H)_6](ClO_4)_6 \cdot 10H_2O$ (**7**) (~0.01 mmol) and excess NEt_4ClO_4 were dissolved in acetonitrile and treated with elemental Br_2(l) in varying mole ratios (1:1, 5:1, 9:1; **9**, **10**, **11**, respectively). An orange-brown solution resulted for **9**, while dark brown solutions were obtained in the other cases. Dark orange crystals were obtained for **9**, while dark brown crystalline solids formed for **10** and **11** in almost quantitative yields. Anal. Calcd for $[Mn_9(C_{19}H_{14}N_9O_2Cl)_6](ClO_4)_6 \cdot 18H_2O$ (**9**): C, 34.00; H, 2.98; N, 18.79%. Found: C, 34.13; H, 2.59; N, 18.46%. Anal. Calcd for $[Mn_9(C_{19}H_{14}N_9O_2Cl)_6](ClO_4)_9 \cdot 14H_2O \cdot 3CH_3CN$ (**10**): C, 32.94; H, 2.71; N, 18.26%. Found: C, 33.32; H, 2.35; N, 17.90%. Anal. Calcd for $[Mn_9(C_{19}H_{14}N_9O_2Cl)_6](ClO_4)_9 \cdot 14H_2O \cdot 3CH_3CN$ (**11**): C, 32.94; H, 2.71; N, 18.26%. Found: C, 32.92; H, 2.29; N, 17.93%.

Crystallographic Data Collection and Refinement of the Structure. The diffraction intensities of an orange-red prismatic crystal of **1** were collected with graphite-monochromatized Mo Kα X-radiation (rotating anode generator) using a Bruker P4/CCD diffractometer at 193(1) K to a maximum 2θ value of 52.9°. The data were corrected for Lorentz and polarization effects. The structure was solved by direct methods.[18,19] All atoms except hydrogens were refined anisotropically. Hydrogen atoms were placed in calculated positions with isotropic thermal parameters set to 20% greater than their bonded partners and were not refined. The partial occupancy of one nitrate was fixed for the final round of refinement. Assuming the normal 2− charge on each ligand, the model is missing two nitrate anions. These are considered to be disordered and indistinguishable within the group of atoms assigned to lattice water. Eight "oxygen" atoms therefore are assumed to represent two nitrate anions. There are 32 hydrogen atoms missing for the model. Neutral atom scattering factors[20] and anomalous-dispersion terms[21,22] were taken from the usual sources. All other calculations were performed with the teXsan[23] crystallographic software. Abbreviated crystal data for **1** are given in Table 1.

Data were collected on a dark red prismatic crystal of **3** using a Nonius Kappa CCD area detector situated at the window of a rotating anode (λ(Mo Kα) = 0.71073 Å). The structures were solved by direct methods, SHELXS-97, and refined using SHELXL-97.[24] Hydrogen atoms were included in the refinement, but thermal parameters and geometry were constrained to ride on the atom to which they are bonded. The data were corrected for absorption effects using SORTAV.[25,26]

(18) (a) SHELX97: Sheldrick, G. M. *SHELX97*; University of Göttingen: Göttingen, Germany, 1997. (b) SIR97: Altomare, A.; Cascarano, M.; Giacovazzo, C.; Guagliardi, A. *J. Appl. Crystallogr.* **1993**, *26*, 343.

(19) DIRDIF94: Beurskens, P. T.; Admiraal, G.; Beurskens, G.; Bosman, W. P.; de Gelder, R.; Israel, R.; Smits, J. M. M. *The DIRDIF-94 program system*; Technical Report of the Crystallography Laboratory; University of Nijmegen: Nijmegen, The Netherlands, 1994.

(20) Cromer, D. T.; Waber, J. T. *International Tables for X-ray Crystallography*; The Kynoch Press: Birmingham, England, 1974; Vol. IV, Table 2.2 A.

(21) Ibers, J. A.; Hamilton, W. C. *Acta Crystallogr.* **1964**, *17*, 781.

(22) Creagh, D. C.; McAuley, W. J. *International Tables for Crystallography*; Wilson, A. J. C., Ed.; Kluwer Academic Publishers: Boston, 1992; Vol C, Table 4.2.6.8, pp 219−222.

(23) *teXsan for Windows: Crystal Structure Analysis Package*; Molecular Structure Corporation: The Woodlands, TX, 1997.

(24) Sheldrick, G. M. *SHELX suite of programs for crystal structure solution and refinement*; University of Göttingen: Göttingen, Germany, 1997.

(25) Blessing, R H. *Acta Crystallogr.* **1995**, *A51*, 33.

(26) Blessing, R. H. *J. Appl. Crystallogr.* **1997**, *30*, 421.

Table 1. X-ray Crystallographic Data for **1**, **3**, **10**

	1	**3**	**10**
empirical formula	$C_{114}H_{122}N_{60}O_{46}Mn_9$	$C_{122}H_{102}Cl_{10}N_{58}O_{56}Mn_9$	$C_{114}H_{84}Cl_{13}N_{54}O_{40}Mn_9$
M	3563.18	4125.58	3805.66
cryst syst	monoclinic	tetragonal	triclinic
space group	$P2_1/n$	$I\bar{4}$	$P\bar{1}$
a/Å	21.308(2)	18.44410(10)	19.1150(10)
b/Å	23.611(2)	18.44410(10)	19.7221(10)
c/Å	32.178(3)	24.9935(3)	26.8334(14)
α/deg	90	90	74.7190(10)
β/deg	93.820(2)	90	77.6970(10)
γ/deg	90	90	64.7770(10)
V/A^3	16153(2)	8502.41(12)	8768.8(8)
ρ_{calcd} (g cm^{-3})	1.465	1.611	1.441
T/K	193(2)	120(2)	120(2)
Z	4	2	2
μ/cm^{-1}	7.73	9.03	9.06
reflns collected			
total, unique, R_{int}	88298, 28408, 0.076	9716, 8476, 0.028	44512, 25082, 0.079
obsd ($I > 3.00\sigma(I)$)	17508	8476	25082
final R1, wR2[a]	0.124, 0.379	0.0604, 0.1684	0.0915, 0.2277

[a] $R1 = \sum||F_o| - |F_c||/\sum|F_o|$, $wR2 = [\sum[w(|F_o|^2 - |F_c|^2)^2]/\sum[w(|F_o|^2)^2]]^{1/2}$.

Data for **9**, **10**, and **11** (**9**, dark brown, 0.10 × 0.06 × 0.02 mm^3; **10**, dark brown, 0.18 × 0.12 × 0.09 mm^3; **11**, dark brown, 0.34 × 0.12 × 0.03 mm^3) were collected with graphite-monochromatized Mo Kα radiation, $\lambda = 0.71073$ Å (Bede Microsource) using a Proteum M diffractometer. The crystals were cooled to 120(1) K using an Oxford Instruments Cryostream.[27] Data were collected to a maximum 2θ value of 52.0°. Data processing was carried out using the SAINT[28a] and XPREP[28b] software packages. Absorption corrections were applied using SADABS.[28c] The structures were solved by direct methods and refined on F^2 using full-matrix least-squares methods within the SHELXTL suite.[28d] Neutral atom scattering factors and anomalous dispersion terms were taken from the usual sources. The SQUEEZE procedure available in the PLATON[29] software was utilized to account for solvent water molecules, for which no suitable structural model could be obtained. Crystal data for **10** are included in Table 1. Crystal data for **9** and **11** are deposited (Table S1).

Structural Descriptions

$[Mn_9(2poap\text{-}2H)_6](NO_3)_6\cdot 14H_2O$ (1). A structural representation for the cation in **1** is shown in Figure 1, and important bond lengths and angles are listed in Table 2. The nine Mn(II) centers are arranged in the familiar grid pattern, common to all the members in this class, with deprotonated hydrazone oxygen atoms bridging all manganese ions. The six ligands are arranged in two roughly parallel groups of three above and below the pseudoplanar metal core, with close contacts between the aromatic rings of 3.7 Å or less indicating significant π contacts between the rings, which clearly stabilize the grid arrangement. The grid can be considered as a roughly flat entity with overall dimensions, including the aromatic hydrogen atoms on the external pyridine rings, of ~20 × 20 Å^2 (2 × 2 nm^2). The structural core showing just the metal ions and the oxygen atoms is shown in Figure 2. Adjacent Mn−Mn distances fall in the range 3.87−4.02 Å, and Mn−O−Mn angles are in the range 125.0−129.5°. Mn−ligand distances are quite variable with long and short contacts (range 2.115−2.387 Å) for the eight

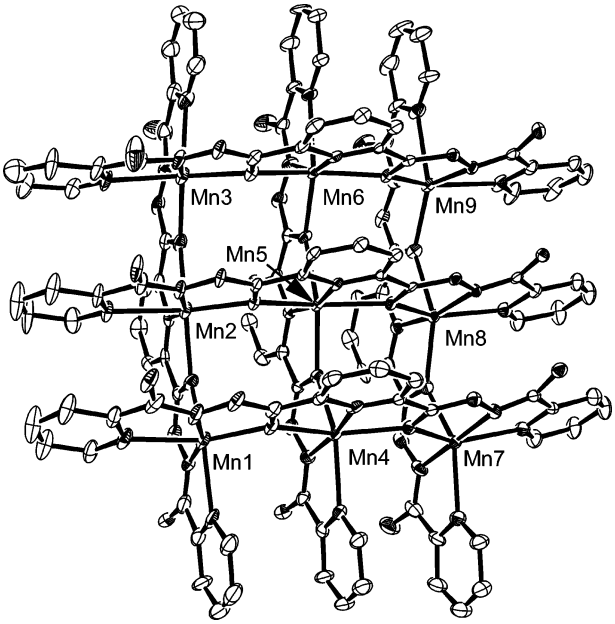

Figure 1. Structural representation for **1** (35% thermal ellipsoids).

Table 2. Bond Distances (Å) and Angles (deg) for **1**

Mn1	N1	2.309(11)	Mn5	O3	2.189(7)
Mn1	N3	2.150(10)	Mn5	O4	2.252(6)
Mn1	N28	2.354(10)	Mn5	O9	2.205(7)
Mn1	N30	2.115(12)	Mn6	N16	2.127(8)
Mn1	O1	2.205(7)	Mn6	N18	2.380(8)
Mn1	O7	2.158(8)	Mn6	N50	2.164(8)
Mn2	N37	2.387(9)	Mn6	O4	2.140(7)
Mn2	N39	2.147(9)	Mn6	O11	2.229(7)
Mn2	N5	2.151(8)	Mn6	O12	2.185(6)
Mn2	O1	2.212(7)	Mn7	N19	2.297(10)
Mn2	O2	2.232(7)	Mn7	N21	2.136(10)
Mn2	O9	2.167(7)	Mn7	N34	2.121(9)
Mn3	N7	2.116(10)	Mn7	N36	2.269(9)
Mn3	N9	2.355(11)	Mn7	O5	2.194(7)
Mn3	N46	2.333(10)	Mn7	O8	2.155(7)
Mn3	N48	2.187(10)	Mn8	N23	2.182(9)
Mn3	O2	2.186(8)	Mn8	N43	2.171(8)
Mn3	O11	2.183(7)	Mn8	N45	2.300(9)
Mn4	N10	2.321(9)	Mn8	O5	2.214(7)
Mn4	N12	2.159(9)	Mn8	O6	2.250(7)
Mn4	N32	2.199(9)	Mn8	O10	2.170(6)
Mn4	O7	2.217(7)	Mn9	N25	2.137(9)
Mn4	O3	2.211(6)	Mn9	N27	2.365(9)
Mn4	O8	2.187(7	Mn9	N52	2.157(8)
Mn5	N14	2.170(8)	Mn9	N54	2.309(9)
Mn5	O10	2.197(6)	Mn9	O6	2.191(7)
Mn5	N41	2.163(7)	Mn9	O12	2.183(7)

Mn1	O1	Mn2	127.9(3)	Mn1	O7	Mn4	126.4(4)
Mn3	O2	Mn2	129.5(3)	Mn7	O8	Mn4	126.7(3)
Mn5	O3	Mn4	128.3(3)	Mn2	O9	Mn5	128.6(3)
Mn6	O4	Mn5	129.8(3)	Mn8	O10	Mn5	125.0(3)
Mn7	O5	Mn8	128.0(3)	Mn3	O11	Mn6	125.1(3)
Mn9	O6	Mn8	129.3(3)	Mn9	O12	Mn6	126.1(3)

(27) Cosier, J.; Glazer, A. M. *J. Appl. Crystallogr.* **1986**, *19*, 105.
(28) (a) Sheldrick, G. M. *SAINTPLUS*, version 6.02; Bruker AXS: Madison, WI, 1997. (b) Sheldrick, G. M. *SHELXS 97, SHELXL 97. Program for the Refinement of Crystal Structures*; University of Göttingen: Göttingen, Germany, 1998. (c) Sheldrick, G. M. *SADABS. Program for Absorption Correction*; University of Göttingen: Göttingen, Germany, 1998. (d) *SHELXTL*, version 5.1; Bruker AXS: Madison, WI. Spek, A. L. *Acta Crystallogr.* **1990**, *A46*, C34.
(29) Spek, A. L. *PLATON—A Multipurpose Crystallographic Tool*; Utrecht Univesity: Utrecht, The Netherlands, 2003.

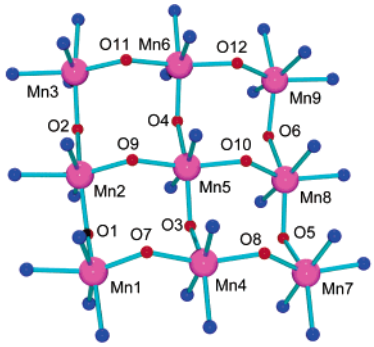

Figure 2. Core structural representation for **1**.

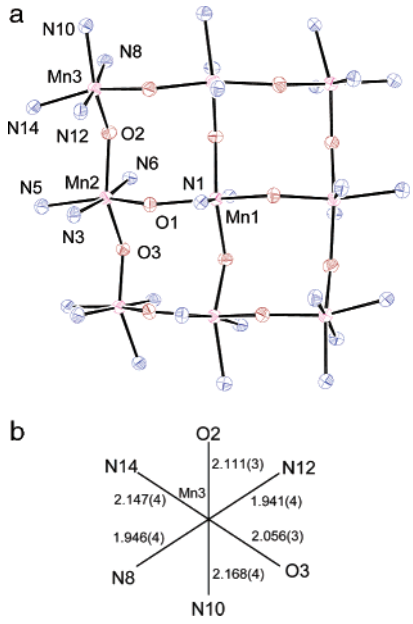

Figure 3. (a) Core structural representation for **3**. (b) Dimensions of a corner Mn(III) center in **3**.

Mn(II) centers in the outer ring. Distances to the peripheral pyridine ring nitrogen atoms fall in the range 2.26−2.39 Å, while other Mn−N and Mn−O distances are considerably shorter. Mn−ligand contacts for the central manganese atom (Mn(5)) are the shortest (2.16−2.26 Å). The large range of distances can be rationalized in terms of the ligands stretching over the $[Mn_9(\mu\text{-}O)_{12}]$ core such that the central metal ion is tightly bound by the congruence of four deprotonated hydrazone oxygen atoms from two ligands, and two nitrogen donor atoms from the central pyridine rings of the same two ligands. The metal atoms in the outer ring are more loosely bound because of a slight mismatch between the ligand dimensions and that of the grid core. The structure of **2** is expected to be the same as that of **1**, on the basis of analytical, spectroscopic, and magnetic data.

$[Mn_9(2poap\text{-}2H)_6](ClO_4)_{10}\cdot 10H_2O$ (3). The overall structure of the cation in **3** is typical of nonanuclear grids in this class, resembling that in **1** and **6**. The core structural representation of **3** is shown in Figure 3a, and relevant bond distances and angles are listed in Table 3. Of immediate significance is the 4-fold rotational symmetry present in the grid, clearly reflecting the equivalence of the four corner manganese centers. Mn(3) metal−ligand distances reveal two

Table 3. Bond Distances (Å) and Angles (deg) for **3**

Mn1	N1	2.219(5)	Mn3	N10	2.168(4)
Mn1	O1	2.233(3)	Mn3	N12	1.941(4)
Mn2	N3	2.115(4)	Mn3	N14	2.147(4)
Mn2	N5	2.312(4)	Mn3	O2	2.111(3)
Mn2	N6	2.159(4)	Mn3	O3	2.056(3)
Mn2	O1	2.149(3)	Mn1	Mn2	3.970(3)
Mn2	O2	2.256(3)	Mn2	Mn3	4.019(3)
Mn2	O3	2.248(3)	Mn2′	Mn3	3.962(3)
Mn3	N8	1.946(4)			

Mn2	O1	Mn1	129.95(13)
Mn3	O2	Mn2	133.94(16)
Mn3	O3	Mn2	133.97(15)

short bonds (Mn(3)−N(12) 1.941(4) Å, Mn(3)−N(8) 1.946(4) Å), and four longer bonds with an average M−L bond distance of 2.062(4) Å. By comparison, Mn(2)−L bond distances are much longer (av 2.207(4) Å). Average Mn(II)−L distances for the equivalent corner atoms in **6** are much longer (2.219(9), 2.200(9), 2.209(8), and 2.216(9) Å).[9] The shorter distances at Mn(3), and at the other symmetry equivalent corner metal ions, indicate a Mn(III) oxidation state for these metal ions, while the side metal atoms and the central Mn atom in **3** (av Mn−L 2.226(4) Å) are clearly Mn(II). For comparison, the averaged equatorial Mn(III)−L distances and Mn(II)−L distances (L = N, O only) in a dinuclear Mn(II)/Mn(III) macrocyclic complex with a $[Mn_2(\mu_2\text{-}O)_2N_4]$ core ($[LMn(II)Mn(III)Cl_2Br]\cdot H_2O$; L = 2:2 macrocycle derived by condensation of 2,6-diformyl-4-*tert*-butylphenol and 1,3-diaminopropane; axial ligands Cl, Br) are 1.97 and 2.23 Å, respectively.[30] Electrochemical oxidation (see Experimental Section) has thus been selective in terms of oxidizing the corner metal centers only.

A close examination of the Mn(3) coordination sphere in **3** (Figure 3b) reveals two "long" bonds (Mn(3)−N(14) and Mn(3)−N(10) > 2.145 Å), and four shorter bonds (<2.12 Å) (Table 3). The long bonds involve terminal pyridine rings on the ligands, which are bound in a *cis* conformation, while the shorter bonds involve the bridging oxygen atoms and the hydrazone nitrogen atoms. The expected elongated Jahn−Teller (JT) axis distortion of high spin octahedral Mn(III) is not observed, but there are two very short bonds (Mn(3)−N(8), Mn(3)−N(12)), which are *trans* to each other.

A survey of a number of typical six-coordinate mononuclear Mn(III) complexes shows that axial elongation is the common way in which the systems distort. [Mn(III)(SABP)(SAL)(MeOH)] (SABP = 2-(salicylideneamino)-4-*tert*-butylphenolate; SAL = deprotonated salicylaldehyde), which has a $MnNO_5$ coordination sphere, has a clearly defined elongated JT axis ($Mn-O_{ax}$ 2.212(4), 2.239(4) Å, O−Mn−O 176.3°; $Mn-L_{eq}$ 1.87−1.99 Å), with four short equatorial contacts.[31] The mononuclear Mn(III) complex $[MnL_2]ClO_4\cdot CH_3OH$ (L = 2-{*N*-[2-(4-imidazolyly)ethyl]-iminomethyl}phenol) has a *trans*-N_4O_2 coordination sphere, two long axial bonds (Mn−N 2.291(6) Å), and much shorter equatorial bonds (Mn−N 2.014(7) Å, Mn−O 1.874(5) Å).[32]

(30) Chang, H.-R.; Larsen, S. K.; Boyd, P. D. W.; Pierpont, C. G.; Hendrickson, D. N. *J. Am. Chem. Soc.* **1988**, *110*, 4565 and references therein.
(31) Mo, S.-J.; Koo, B.-K. *Bull. Korean Chem. Soc.* **1999**, *20*, 1225.

The mononuclear complex $[MnL(H_2O)_2]Cl_3 \cdot 2H_2O \cdot 0.5HCl$ (L = tetraaza-macrocyclic ligand) has a similar *trans*-N_4O_2 coordination sphere, with axially elongated Mn−O contacts (Mn−O 2.179(1) Å) and four short equatorial Mn−N contacts (2.036(2), 2.069(2) Å).[33] The complex $[Mn(bzacen)(MeOH)_2]ClO_4$ ($bzacen^{2-}$ = *N*,*N*′-ethylenebis(1-phenyl-3-imino-1-butanoato)) has an axially elongated *cis*-N_2O_4 structure with long axial Mn−O contacts (2.294(5), 2.296(5) Å) and much shorter equatorial contacts (Mn−N 1.970(6), 1.958(6) Å; Mn−O 1.882(5), 1.884(4) Å).[34]

Two unusual complexes $[Mn(sal\text{-}N(1,5,8,12))]ClO_4$ and $[Mn(3\text{-methoxy-sal-}N(1,5,8,12))]ClO_4 \cdot H_2O$ (ligands derived from *N*,*N*′-bis(3-aminopropyl) ethylenediamine and salicylaldehyde and 3-methoxy salicylaldehyde, respectively) have distorted *trans*-MnN_4O_2 coordination spheres, but with long Mn−N (amine) contacts (2.239(5), 2.207(4) Å and 2.163(2), 2.174(2) Å, respectively) in a *cis* orientation. The remaining bonds (1.869−2.102 and 1.869−2.104 Å, respectively) are much shorter. However, in both of these complexes there are two quite short Mn−O bonds in a *trans* orientation (1.869(4), 1.878(4) Å and 1.869(2), 1.873(2) Å respectively), which may indicate that the preferred distortion could be a possible JT compression.[35] Another example with longer *cis* Mn(III)−N (amine and imine) bonds (2.23(1), 2.18(1) Å) is the phenoxo-bridged mixed valence Mn(II)/Mn(III) complex $[Mn_2(bcmp)(\mu\text{-}OAc)_2](ClO_4)_2$ (bcmp = 2,6-bis(1,4,7-triazacyclonon-1-ylmethyl)-4-methylphenol), which involves a *fac*-N_3O_3 coordination sphere.[36]

The absence of an elongated JT axis in **3** is considered to be the consequence of the way in which the six ligands stretch over the grid arrangement of the nine metal ions. The long external *cis*-bonds in **3** (Mn(3)−N(14) 2.147(4) Å, Mn(3)−N(10) 2.168(4) Å), which involve the peripheral pyridine rings, are typical of the [3 × 3] grids in general but occur regardless of the metal ion and its oxidation state. This appears to be a consequence of the constraints brought to bear by the congruence of the six ligands, and the balance of ligand strain and electrostatic forces associated with the overall grid structure. The expected axially elongated Mn(III) JT distortion in **3** appears therefore to be compromised in favor of other steric factors. However, there are two short *trans* contacts (Mn(3)−N(12) 1.941(4) Å, Mn(3)−N(8) 1.946(4) Å).

A comparison of **3** with the parent complex **6** reveals some other interesting geometric consequences of the oxidation. The overall grid core dimensions in **6** show corner to corner Mn−Mn separations of 7.880(3), 7.757(3), 7.775(3), and 7.810(3) Å (av 7.806 Å), with Mn−O−Mn angles in the range 125.9−130.7° (av 127.9°).[9] Surprisingly, the overall core size in **3** is slightly larger with a Mn−Mn distance of 7.934 Å. This can be rationalized in terms of larger Mn−O−Mn angles in **3**, which fall in the range 129.95−133.97° (av 132.62°), despite the average shortening of the bonds to the corner atoms. The average Mn−Mn distance in **3** (3.984(3) Å) is also slightly larger than that in **6** (3.944(6) Å).

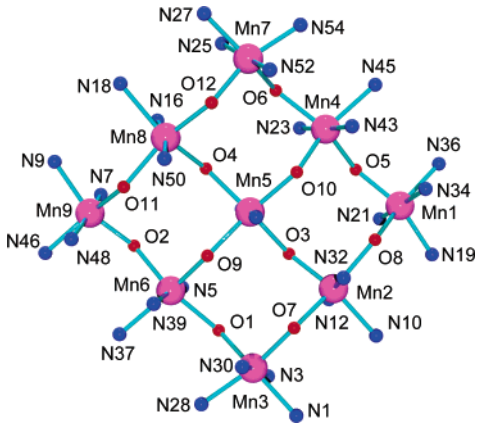

Figure 4. Core structural representation for **10**.

$[Mn_9(Cl2poap\text{-}2H)_6](ClO_4)_6 \cdot 18H_2O$ (9), $[Mn_9(Cl2poap\text{-}2H)_6](ClO_4)_9 \cdot 14H_2O \cdot 3CH_3CN$ (10), $[Mn_9(Cl2poap\text{-}2H)_6](ClO_4)_9 \cdot 14H_2O \cdot 3CH_3CN$ (11). Structural information was obtained for several oxidized samples produced by treatment of $[Mn_9(Cl2poap\text{-}2H)_6](ClO_4)_6 \cdot 10H_2O$ (**7**) with Br_2/CH_3CN in varying ratios (1:1, 5:1, 9:1; see Experimental Section). In all three cases, the grid remains intact on reaction with bromine, and the only significant differences in the structures relate to the dimensions of the corner manganese atoms. An examination of the average bond distances at the corner Mn centers in **9** (Mn(1) 2.198(9) Å, Mn(3) 2.168(9) Å, Mn(7) 2.213(8) Å, Mn(9) 2.183(9) Å) suggests that little oxidation, if any, has occurred. For comparison, the average distances for the corner metal ions in the starting material **7** are 2.213(5), 2.226(5), 2.209(5), and 2.229(5) Å.[17] Considering the esd's on the distances, the corner Mn centers are considered to be effectively unchanged. This is consistent with the magnetic properties (vide infra), and the fact that only 1 equiv of Br_2 was added, which appears not to have had a significant oxidation effect.

The core structure of **10** is shown in Figure 4, and selected bond distances and angles are listed in Table 4. The structure and the crystallographic parameters bear a close resemblance to the previously reported compound $[Mn_9(Cl2poap\text{-}2H)_6](ClO_4)_9 \cdot 7H_2O$ (**8**), produced by reaction of **7** with saturated chlorine water.[17] There are slight differences in the cell parameters, but the refinement is considerably better in the present case. Average Mn−L distances for the corner atoms in **10** are quite short (Mn(1) 2.069(7) Å, Mn(3) 2.102(7) Å, Mn(7) 2.069(7) Å, Mn(9) 2.091(8) Å) and comparable with those for **8** (2.055(8), 2.066(7), 2.096(10), 2.164(8) Å). The assessment of the metal ion oxidation state can be based on the corner Mn−L distances observed for **3** (av 2.062(4) Å), and **7** (vide supra), which suggests that for **8** three metal ions are fully oxidized.[17] For **10**, it is likely that Mn(1), Mn(7), and Mn(9) are Mn(III). However, given the fairly short overall distances to Mn(3), the possibility of partial

(32) Mikuriya, M.; Nukada, R.; Tukami, W.; Hashimoto, Y.; Fujii, T. *Bull. Chem. Soc. Jpn.* **1996**, *69*, 1573.
(33) Kim, J. C.; Lough, A. J. *Bull. Korean Chem. Soc.* **1999**, *20*, 1241.
(34) Liu, S.-X.; Feng, Y.-L. *Polyhedron* **1996**, *15*, 4195.
(35) Panja, A.; Shaikh, N.; Gupta, S.; Butcher, R. J.; Banerjee, P. *Eur. J. Inorg. Chem.* **2003**, 1540.
(36) Diril, H.; Chang, H.-R.; Nilges, M. J.; Zhang, X.; Potenza, J. A.; Schugar, H. J.; Isied, S. S.; Hendrickson, D. N. *J. Am. Chem. Soc.* **1989**, *111*, 5102.

Table 4. Bond Distances (Å) and Angles (deg) for **10**

Mn1	N21	1.938(8)	Mn5	O9	2.227(7)
Mn1	N34	1.976(9)	Mn5	N14	2.231(8)
Mn1	O5	2.052(6)	Mn5	O3	2.250(6)
Mn1	O8	2.103(7)	Mn6	N39	2.129(10)
Mn1	N36	2.165(5)	Mn6	O9	2.150(7)
Mn1	N19	2.181(4)	Mn6	N5	2.171(10)
Mn2	N12	2.092(8)	Mn6	O2	2.240(8)
Mn2	O3	2.134(7)	Mn6	O1	2.241(7)
Mn2	N32	2.182(8)	Mn6	N37	2.350(4)
Mn2	O7	2.216(7)	Mn7	N52	1.956(11)
Mn2	O8	2.238(6)	Mn7	N25	1.981(9)
Mn2	N10	2.275(4)	Mn7	O12	2.043(7)
Mn3	N30	1.992(9)	Mn7	N54	2.105(6)
Mn3	N3	2.009(9)	Mn7	O6	2.137(7)
Mn3	O7	2.088(7)	Mn7	N27	2.192(4)
Mn3	O1	2.140(7)	Mn8	N16	2.112(10)
Mn3	N28	2.172(6)	Mn8	N50	2.134(10)
Mn3	N1	2.213(6)	Mn8	O4	2.160(6)
Mn4	N43	2.117(9)	Mn8	O11	2.219(8)
Mn4	N23	2.155(8)	Mn8	O12	2.220(8)
Mn4	O10	2.159(7)	Mn8	N18	2.407(4)
Mn4	O6	2.214(6)	Mn9	N48	1.978(13)
Mn4	O5	2.242(6)	Mn9	N7	1.984(11)
Mn4	N45	2.331(4)	Mn9	O2	2.065(7)
Mn5	N41	2.217(9)	Mn9	O11	2.116(9)
Mn5	O4	2.221(7)	Mn9	N9	2.186(5)
Mn5	O10	2.222(7)	Mn9	N46	2.218(5)

Mn3	O1	Mn6	131.4(4)	Mn3	O7	Mn2	133.3(4)
Mn9	O2	Mn6	132.0(5)	Mn1	O8	Mn2	134.7(4)
Mn2	O3	Mn5	128.9(4)	Mn6	O9	Mn5	128.4(4)
Mn8	O4	Mn5	129.1(4)	Mn4	O10	Mn5	129.2(4)
Mn1	O5	Mn4	132.3(4)	Mn9	O11	Mn8	133.8(5)
Mn7	O6	Mn4	133.2(4)	Mn7	O12	Mn8	133.1(5)

oxidation at this site cannot be excluded. The Mn−L distances at the other noncorner metal centers are much larger, and typical of Mn(II).

An examination of the corner sites in **10** in more detail shows that Mn(1) and Mn(9) have long Mn−N (pyridine) bonds (N(19), N(36) and N(9), N(46), respectively), which are arranged *cis*, as in **3**. Therefore, it is difficult to define a normal JT axis. A similar *cis* arrangement of long Mn−N (pyridine) bonds is observed for Mn(3) (N(1), N(28)), which is not considered to be fully oxidized. However, Mn(7) has short overall Mn−L contacts, indicative of Mn(III), but surprisingly two long *trans* bonds (Mn(7)−O(6) 2.137(7) Å, Mn(7)−N(27) 2.192(4) Å), and four much shorter equatorial bonds, typical of an axially elongated Mn(III) center. Compound **8** has a similar *trans* elongation at one Mn(III) site.[17] This suggests that there is a subtle balance of effects which control the corner metal ion site geometries. The overall state of oxidation of the corner metal ions in the grid would control the Mn−L bond lengths, which would tend to pull the ligands toward the core and create ligand strain. In the case of compound **3** with four Mn(III) centers, this leads to the unusual *cis* arrangement of the long Mn(III)−L bonds. For compounds **8** and **10**, with one more Mn(II) center on average, and longer overall Mn−L bonds, the grid can relax a little, and this may allow one Mn(III) ion to exhibit a typical axial JT elongation.

The cell dimensions for **11** (Table S1) are almost the same as those for **10**, with the same space group, and the corner Mn−L distances are all quite short (Mn(1) 2.049(8) Å, Mn(3) 2.056 Å, Mn(7) 2.047(8) Å, Mn(9) 2.067(8) Å), all of which would be typical of Mn(III). These results present a fundamental conundrum concerning the unique geometric situation which a molecular square grid array of nine approximately equivalent Mn(II) centers provides. The four corner centers each oxidize in a one-electron step at essentially the same potential (0.63 V vs Ag/AgCl; vide infra), as indicated by the electrochemistry results, and so, the removal of four electrons is largely dependent upon both the oxidation potential of the oxidant and the amount present. The standard reduction potential for bromine (aqueous vs NHE) is 1.065 V, which should be sufficient to oxidize all four corner Mn(II) centers to Mn(III). However, the increasing positive charge on the grid cation, which results as oxidation proceeds, suggests the necessity for a large excess of oxidant for complete corner metal ion oxidation.

The dimensions of the corner Mn atoms in **11** do indeed suggest that full corner oxidation has occurred. However, the crystal used for a structural analysis is not necessarily representative of a bulk sample, and so in this case an independent assessment of the bulk oxidation state is required. Magnetic measurements can provide this (vide infra) and indicate that on average only three corner sites are oxidized. Also, a comparison between **8**, **10**, and **11** reveals that differing degrees of oxidation may exist at some corner manganese sites as indicated by average Mn−L distances, which are between those expected for Mn(II) and Mn(III) in the current grid systems (e.g., 2.164(8) Å (**8**) and 2.102(8) Å (**10**)). This would result in a very small change in electron density from one crystalline sample to the next and lead to a very small change in the crystallographic cell dimensions of **10** and **11**. This might suggest that a "superlattice" approach to a crystallographic evaluation of the problem could provide a better picture of the oxidized grids, particularly for **10** and **11**.

The structural results are, however, consistent with the stoichiometric ratio of Br_2(l)/grid complex, and the match of potentials for the grid and the oxidant, in that increased overall oxidation of the corner sites only occurs with increasing bromine concentration. However, complete corner site oxidation has thus far been achieved more successfully using a bulk electrolytic approach.

Electrochemical Measurements. Cyclic voltammetry was carried out on $[Mn_9(M2poap\text{-}2H)_6](ClO_4)_6\cdot 22H_2O$ (**2**) (red), $[Mn_9(2poap\text{-}2H)_6](ClO_4)_6\cdot 18H_2O$ (**6**) (green),[9] and $[Mn_9(Cl2poap\text{-}2H)_6](ClO_4)_6\cdot 10H_2O$ (**7**) (black)[14] in acetonitrile (0.1 M TEAP) (Figure 5). In all cases, five waves are observed in the potential range 0.5−1.65 V (vs Ag/AgCl), with a high current wave in the range 0.5−0.9 V, followed by four lower current waves at higher potential. Coulometric measurements show that the first wave in each case corresponds to a four-electron oxidation process, while the four higher potential waves are single-electron redox events. In each case, the waves are associated with Mn(II) ↔ Mn(III) redox processes, with four Mn(II) centers being oxidized in the first major wave at approximately the same potential. ΔE_p values for this wave (216, 201, 153 mV, respectively) suggest a quasireversible redox process. ΔE_p values for the remaining four waves are much smaller and indicative of

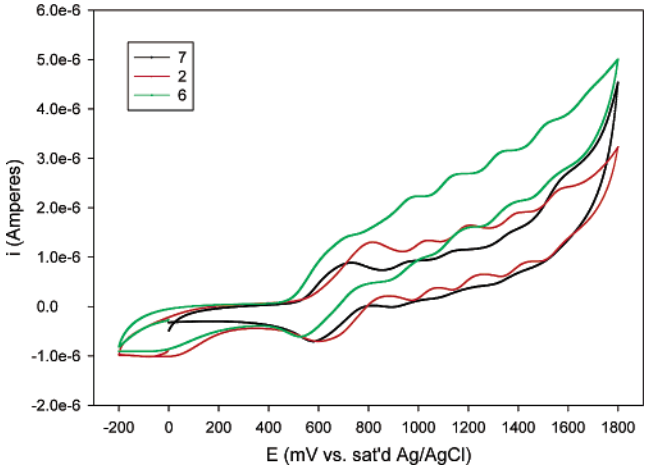

Figure 5. Cyclic voltammetry for **2**, **6**, and **7** ($\sim 1 \times 10^{-3}$ M + 0.1 M NEt_4ClO_4; potentials versus Ag/AgCl).

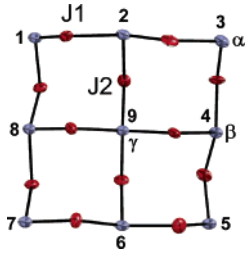

Figure 6. Core grid model.

more reversible redox processes. The broad first wave (0.5−0.9 V) is associated with the oxidation of four corner Mn(II) centers (Figure 6; α sites), while the subsequent higher potential waves are assigned to Mn(II) centers on the sides of the grid (Figure 6; β sites). No further oxidation waves are observed in the $Mn(II)_9$ systems, which could be associated with the central metal ion. The potential cutoff using a platinum working electrode is around 1.8 V (vs Ag/AgCl). The *trans*-N_2O_4 coordination environment for the central metal ion might suggest oxidation within the potential range examined, but the special, protected position of this site might lead to unusual stability of the Mn(II) state.

While cyclic voltammetry gives a clear indication of the separate redox processes, differential pulse voltammetry (DPV) is a potentially more sensitive technique capable of resolving minute differences in oxidative potentials.[37] DPV highlights the individual redox responses much more clearly (Figure 7; high (50 mV) pulse amplitude for **2**, **6**, and **7**). A broad peak (I) is observed in the range 0.55−0.75 V, corresponding to the comparable broad wave in CV for oxidation of the α centers, and four distinctive one-electron peaks are observed between 0.9 and 1.65 V (peaks II−V) in each case, corresponding to the oxidation of the β centers. The first oxidation occurs at different potentials, in the sequence **2** < **7** < **6**, corresponding to $Mn(II)_9$ grids with MeO, Cl, and H groups on the 4-positions of the central pyridine rings, respectively. The positions of the subsequent higher potential waves vary also. There is clearly an

(37) Bard, A. J.; Faulkner, L. R. *Electrochemical Methods: Fundamentals and Applications*, 2nd ed.; New York: John Wiley & Sons Inc., 2001.

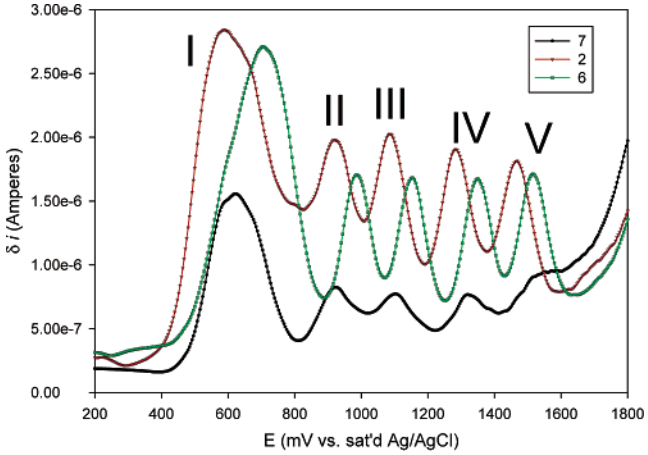

Figure 7. Differential pulse voltametry for **2**, **6**, and **7** (20 mV/s scan rate, 50 mV pulse amplitude, 50 ms pulse width; potentials vs Ag/AgCl).

Table 5. Electrochemical Data for Compounds **2**, **6**, and **7**

comproportionation process	$\Delta E_{1/2}$ (±10 mV)	K_{com}
$[\mathbf{6}]^{10+} + [\mathbf{6}]^{12+} = 2[\mathbf{6}]^{11+}$	168	700
$[\mathbf{6}]^{11+} + [\mathbf{6}]^{13+} = 2[\mathbf{6}]^{12+}$	194	1900
$[\mathbf{6}]^{12+} + [\mathbf{6}]^{14+} = 2[\mathbf{6}]^{13+}$	168	700
$[\mathbf{2}]^{10+} + [\mathbf{2}]^{12+} = 2[\mathbf{2}]^{11+}$	166	600
$[\mathbf{2}]^{11+} + [\mathbf{2}]^{13+} = 2[\mathbf{2}]^{12+}$	198	2200
$[\mathbf{2}]^{12+} + [\mathbf{2}]^{14+} = 2[\mathbf{2}]^{13+}$	184	1300
$[\mathbf{7}]^{10+} + [\mathbf{7}]^{12+} = 2[\mathbf{7}]^{11+}$	171	800
$[\mathbf{7}]^{11+} + [\mathbf{7}]^{13+} = 2[\mathbf{7}]^{12+}$	240	11500
$[\mathbf{7}]^{12+} + [\mathbf{7}]^{14+} = 2[\mathbf{7}]^{13+}$	114	90

electronic influence associated with the substituent on the 4-position of the central pyridine ring, which is communicated to all the metal ions in the grid. In the case of **2**, a general decrease in wave potential would be consistent with charge delocalization from a 4-methoxy group into the grid, and redistribution through the Mn−O−Mn framework.

The potential at which a maximum current response is achieved (E_{max}) is related to the half-wave potential by the following relationship (eq 1):

$$E_{max} = E_{1/2} - \frac{E_{pulse}}{2} \qquad (1)$$

Thus, from a typical DPV experiment (Figure 7; E_{pulse} equal to 50 mV) half-wave potentials can be calculated and compared with a fair degree of reliability (Table 5). Using methods developed by Richardson and Taube,[38] comproportionation constants (K_{com}) can also be extracted from the DPV analysis. This assumes a reaction of the type

$$A \xrightarrow{n_1, E_1^\circ} B \xleftarrow{n_2, E_2^\circ} C$$

with an equilibrium constant K_{com} (eq 2).

$$K_{com} = \frac{[B]^{(n_1+n_2)}}{[A]^{n_1}[C]^{n_2}} = e^{[(E_1^\circ - E_2^\circ)n_1 n_2 F/RT]} \qquad (2)$$

In this case, the value of ΔE° is determined via DPV

(38) Richardson, D. E.; Taube, H. *Inorg. Chem.* **1981**, *20*, 1278.

measurement, since it is related to the half-wave potential by the following relationship (eq 3):

$$E^\circ = E_{1/2} - \left(\frac{RT}{nF}\right)\ln\left[\left(\frac{f_O}{f_R}\right)\sqrt{\frac{D_R}{D_O}}\right] \quad (3)$$

Assuming that the diffusion and activity coefficients do not differ significantly between the oxidized and reduced forms (a reasonable assumption in this case), the redox potentials can be approximated by the half-wave potentials, i.e.

$$E^\circ \approx E_{1/2} \quad (4)$$

Utilizing the approximation in eq 4 and evaluating eq 2 at 298 K for $n_1 = n_2 = 1$ yields

$$K_{com} = e^{[\Delta E_{1/2}/25.68mV]} \quad (5)$$

Since the peak separations for the final four oxidation waves in **2** and **6** are for the most part between ca. 165 and 200 mV, the peak currents are well resolved. Thus, eq 1 applies, and $\Delta E_{1/2}$ is given by ΔE_{peak}. The data for **7** are somewhat unreliable, and separation of the last two peaks is less than ideal; however, for the sake of comparison, comproportionation constants were calculated regardless. Peak separations and comproportionation constants for **2**, **6**, and **7** are listed in Table 5.

These K_{com} values (<12000) are quite small, and much smaller than those reported for a number of macrocyclic diphenoxide bridged complexes $[LM_2(\mu\text{-}O)_2]$ (M = Mn, Cu), which have values on the orders 10^{10-11} and 10^6, respectively.[30] This indicates that the individual mixed oxidation state intermediates ($[grid]^{11+}$, $[grid]^{12+}$, $[grid]^{13+}$), which occur during the sequence of four one-electron oxidation steps, are not very stable compared with their redox counterparts, and that there is little charge delocalization, suggesting weakly interacting class 2 behavior.

Visible and Near-Infrared Absorption Spectroscopy. Coulometric oxidation and chemical oxidation lead to distinctive color changes, from yellow-orange solutions of the $Mn(II)_9$ complexes to deep brown solutions of the mixed oxidation state systems. Figure 8 illustrates the absorption spectrum in solution (CH_3CN) for **3**, **4**, and **6** in the 7000−17000 cm^{-1} region. The unoxidized complex **6** (black) shows essentially a baseline response in this range, with no significant absorption, typical of Mn(II). Two prominent, new, and moderately intense bands appear on oxidation at ~10000 and ~14300 cm^{-1}, and grow in intensity as oxidation proceeds. Compound **4** has three corner Mn(II) centers oxidized $[Mn(III)_3Mn(II)_6]$ (vide infra) and is identical to **8**, which has been previously reported.[17] Compound **3** is an example of a $[Mn(III)_4Mn(II)_5]$ system, where all four corner α Mn(II) centers are oxidized to Mn(III). The bands appear at approximately the same wavelengths for both compounds, but the increase in extent of oxidation is clearly responsible for the significant increase in absorption intensity (400−800 M^{-1} cm^{-1}), implying that their origin is associated with the presence of an increasing number of Mn(III) sites. A similar increase in the intensity of these bands is observed

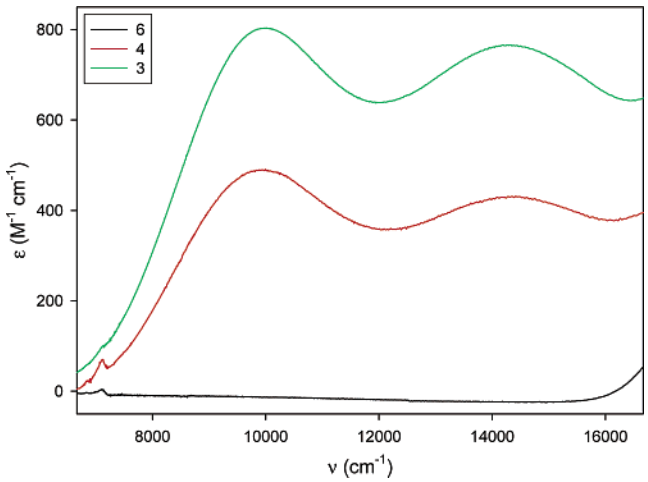

Figure 8. Visible and near-IR absorption spectra (CH_3CN) for **3**, **4**, and **6**.

on incremental addition of Cl_2(aq) to an acetonitrile solution of compound **6**. The absorption intensities are fairly large, but for **3** are of the order of 200 M^{-1} cm^{-1} per Mn(III) ion. This is not considered to be too large to be associated with nominally Laporte forbidden d−d transitions for octahedral Mn(III). An examination of some Mn(III) mononuclear complexes with chromophores in the series MnO_6, MnN_2O_4, and MnN_3O_3 reveals that the longest wavelength absorption is for $[Mn(III)(DMSO)_6](ClO_4)_3(CH_3CN)$ (640 nm; $\epsilon = 230$ M^{-1} cm^{-1}). With increased nitrogen donor content, λ_{max} shifts to shorter wavelengths, with comparable intensities.[39] The mixed oxidation state Mn(II)/Mn(III) complexes $[Mn_2(bpmp)(\mu\text{-}OAc)_2](ClO_4)_2$ and $[Mn_2(bcmp)(\mu\text{-}OAc)_2](ClO_4)_2$[36] (vide supra) have visible absorptions in the ranges 450−480 and 590−630 nm, with intensities in the range $\epsilon = 600-1200$ M^{-1} cm^{-1}. Despite the high intensities, these are assigned as ligand field bands associated with the *cis*-$Mn(III)N_3O_3$ centers.

The *cis*-$Mn(III)N_4O_2$ coordination sites at the oxidized corner grid positions would be expected to have d−d transitions at shorter wavelengths than the examples quoted above, because of the increased nitrogen donor content. The observed bands for **3** and **4** appear at 700 and 1000 nm (~14300 and 10000 cm^{-1}, respectively), with intensities up to 800 M^{-1} cm^{-1}. By comparison with other Mn(III) systems, these bands are considered to be at wavelengths which are too long to be ligand field (d−d) transitions and are therefore associated with charge transfer transitions.

The electron dynamics of the charge delocalization in **3** have been analyzed in a separate study,[40] using a typical Marcus−Hush approach, which reveals that the 10000 cm^{-1} absorption is likely to be LMCT ($(\mu\text{-}O) \rightarrow Mn(III)$) in nature, while the absorption at 14300 cm^{-1} appears to be an intervalence charge transfer (IVCT) band. A preliminary spectroelectrochemical study has also been carried out on an acetonitrile solution of the $Mn(II)_9$ complex **6**, by first

(39) Yamaguchi, K.; Sawyer, D. T. *Inorg. Chem.* **1985**, *24*, 971 and references therein.
(40) Thompson, D. W.; Kelly, T. L.; Thompson, L. K.; Dawe, L. N. Manuscript in preparation.

setting the potential at 0.9 V(vs Ag/AgCl) and oxidizing until the four corner sites were converted to Mn(III), and then resetting the potential to 1.7 V (vs Ag/AgCl), while monitoring the visible/near-infrared absorption. A growth of the two bands at 700 and 1000 nm was observed at 0.9 V, with maximum absorbance corresponding to passage of four electron equivalents. Further oxidation at higher potential resulted in the gradual lowering in intensity of the 700 nm band, and an increase in intensity of the 1000 nm band, which shifts to slightly shorter wavelength. This suggests that the 700 nm band is IVCT in nature. Full details of the spectroelectrochemistry and Marcus−Hush analysis will appear elsewhere.[40] Addition of ascorbate to the oxidized species reverses the color change of the oxidized solutions from brown back to yellow-orange, with complete disappearance of the charge transfer bands, and reversion to the baseline spectrum. This clearly indicates that these bands are associated with the presence of the Mn(III) centers.

Magnetic Properties of Oxidized Grids. An in-depth assessment of the magnetic properties of the $Mn(II)_9$ grid systems, which have a total of 45 "d" electrons, is complicated by the enormous dimension of the Hilbert space required for a full analysis of the isotropic exchange problem (∼60 GB of RAM required). Compound **6** has been studied by inelastic neutron scattering revealing an $S = {}^5/_2$ ground multiplet, with lowest lying excited-state multiplets of $S = {}^7/_2$, $S = {}^3/_2$, $S = {}^3/_2$, and $S = {}^9/_2$ in increasing order of energy. The analysis was carried out using irreducible tensor operator theory, and the exact Lanczos algorithm.[41] A recent approach to a simplification of the $Mn(II)_9$ case involves considering the outer ring of eight Mn(II) centers as a chain ($n = 8$).[17] This is regarded as reasonable, given that the ground state for all examples in this class was found to be $S = {}^5/_2$, and that J2 was considered to be small compared with J1 (Figure 6). J1 was evaluated for several grids from a normal chain expression involving $S = {}^5/_2$ spin centers, giving good data fits, and values ($-J1 = 4-5$ cm^{-1}) comparable with that obtained using D_4 permutational symmetry for compound **6**.[12]

A mixture of Mn(II) and Mn(III) sites in the outer ring of the grid presents additional challenges for evaluation of the exchange problem, despite the large dimensions of any calculations. Even with imposed D_4 rotational symmetry, the calculation of the spin state manifold for a $Mn(II)_9$ grid would require ∼4 GB of RAM, and significant computational expense. However, by reducing the total electron complement of the grid the full isotropic exchange situation for a smaller spin system, e.g., $(d^3)_9$, can be evaluated with relative ease, and trends compared usefully with the Mn(II)/Mn(III) systems.

$$H_{ex} = -J1\left(\sum_{i=1-7} S_i \cdot S_{i+1} + S_8 \cdot S_1\right) - J2(S_2 + S_4 + S_6 + S_8) \cdot S_9 \quad (6)$$

The isotropic exchange Hamiltonian (eq 6) defines the two exchange integrals in the grid composed of a ring of eight spin centers (S_1-S_8; J1) coupled to the central spin center (S_9; J2) (Figure 6). The total spin states (S') and their energies have been evaluated using normal procedures, and substituted into the van Vleck equation using MAGMUN4.0,[42] in order to calculate variable temperature magnetic profiles for varying S values. Figure 9 shows the variable temperature magnetic profile for a grid with $S = {}^2/_2$ centers at the corners, and $S = {}^3/_2$ centers elsewhere (S_1, S_3, S_5, $S_7 = {}^2/_2$; Figure 6, $\beta = \gamma = d^3$, $\alpha = d^2$) with $g = 2.0$, $J1 = J2 = -17.5$ cm^{-1} (chosen arbitrarily). χ_{mol} gradually increases as temperature is lowered, reaching a pronounced maximum at ∼55 K, with a rapid rise at low temperatures. The magnetic moment per mole drops from 9.2 μ_B at 300 K to 1.73 μ_B at 2 K. This corresponds to a ferrimagnetic ($4 \times S = {}^1/_2$) subunit in the outer ring of eight centers, resulting from the intraring antiferromagnetic exchange, which then couples with the central $S = {}^3/_2$ spin center antiferromagnetically leading to an $S = {}^4/_2 - {}^3/_2 = {}^1/_2$ ground state. If J2 is set to zero, no maximum in χ is observed, and the ground state becomes $S = {}^4/_2 + {}^3/_2$, with a moment at 2 K of 6.2 μ_B. Setting S_1 and $S_3 = {}^2/_2$ and all other spin centers to ${}^3/_2$ with $J1 = J2 = -17.5$ cm^{-1} creates a similar χ/T profile but generates the opposite situation, and the ground state now becomes $S = {}^3/_2 - {}^2/_2 = {}^1/_2$, which is the same as before, with a moment at 2 K of 1.73 μ_B.

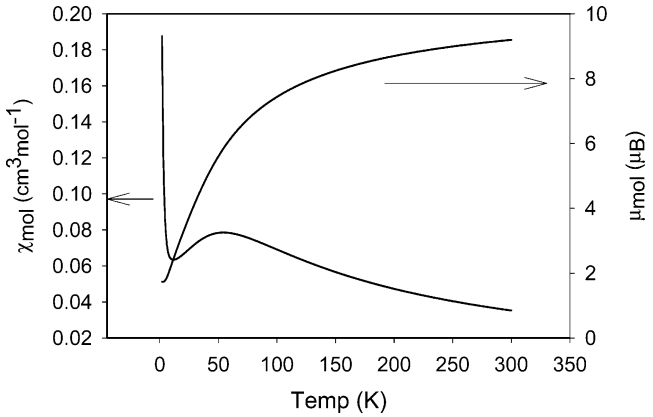

Figure 9. Variable temperature magnetic properties for a $(d^2)_4(d^3)_5$ model grid ($g = 2.0$, $J1 = J2 = -17.5$ cm^{-1}).

Compound **4**, which is produced by electrochemical oxidation of **7**, has a profile of magnetic susceptibility (per mole) (Figure 10) which has a pronounced shoulder at ∼40 K, followed by a sharp rise at lower temperature. This is a clear signature of intramolecular antiferromagnetic exchange coupling for a $[Mn(III)_3Mn(II)_6]$ system in which all manganese centers are involved in spin exchange throughout the grid and is identical to the behavior of **8**, which has been reported elsewhere.[17] The moment at room temperature (14.9 μ_B) is consistent with a "42" electron system with three Mn(III) centers. The value at 2 K (3.5 μ_B) is close to what would be expected for a system with an $S = {}^2/_2$ ground state, with global antiferromagnetic exchange. A comparison with

(41) Guidi, T.; Carretta, S.; Santini, P.; Liviotti, E.; Mondelli, C.; Waldmann, O.; Thompson, L. K.; Zhao, L.; Frost, C. D.; Amoretti, G.; Caciuffo, R. *Phys. Rev. B* **2004**, *69*, 104432.

(42) MAGMUN4.0 is available free of charge through http://www.chem-.mun.ca/resinst/. The programs may be used only for scientific purposes, and economic utilization is not allowed. If the routine is used to obtain scientific results, which are published, the origin of the program should be quoted.

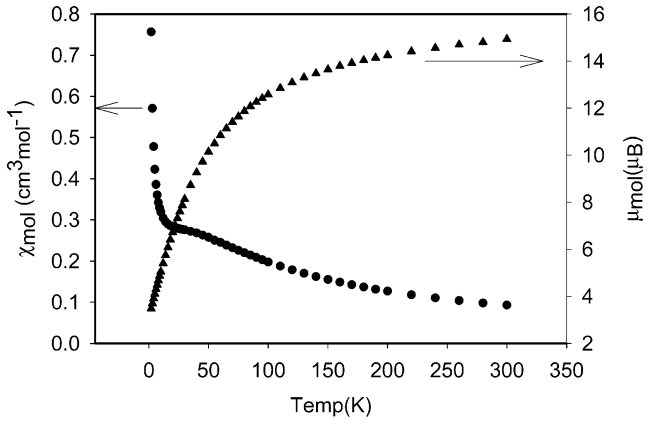

Figure 10. Magnetic profiles for **4** (χ_{mol}/T, μ_{mol}/T).

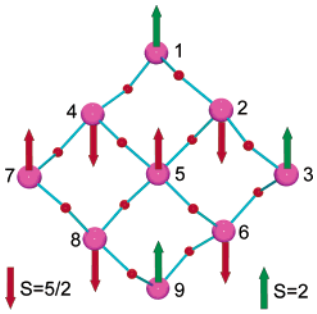

Figure 11. Spin model for **4**.

Figure 9 for the model d^3/d^2 grid system indicates that antiferromagnetic exchange in the outer ring leads to a noncompensation of spins, and a ferrimagnetic $S = 3 \times {}^1/_2$ situation. This spin subunit then undergoes antiferromagnetic exchange with the central Mn(II) leading to an $S = {}^5/_2 - {}^3/_2 = {}^2/_2$ ground state. Magnetization studies as a function of field at 2 K confirm this and are identical to those reported previously.[17] Figure 11 illustrates a spin dipole model describing the overall exchange situation. In this case, the intramolecular coupling scheme must involve J1 and J2 values of comparable magnitude, and it is reasonable to assume that they will be similar to those obtained for the $Mn(II)_9$ systems (J1 ≈ -5 cm^{-1}),[14,17] given the similar Mn−O−Mn angles.

Compound **3**, which has a [α(III)$_4$β(II)$_4$γ(II)] (Figure 6) distribution of manganese centers, has a superficially similar magnetic profile (Figure 12) but with a clearly defined maximum in χ_{mol} at a higher temperature (55 K). The moment value at 2 K (1.83 μ_B) is indicative of an $S = {}^1/_2$ ground state system, which is supported by *M*/*H* data at 2 K (Figure S1). The room temperature moment is reasonable for a system with 41 unpaired electrons. The magnetic properties are a clear signature of exchange throughout the whole grid, with antiferromagnetic coupling between the eight metal centers in the outer ring leading to an $S = 4 \times {}^1/_2$ "ferrimagnetic" ground state for the ring. The ring then couples antiferromagnetically to the central Mn(II) site leading to an overall ground state of $S = {}^5/_2 - {}^4/_2 = {}^1/_2$, consistent with the d^3/d^2 model and the properties of **4**. Compound **5** has essentially identical magnetic properties, indicating a similar distribution of Mn(III) centers, as would

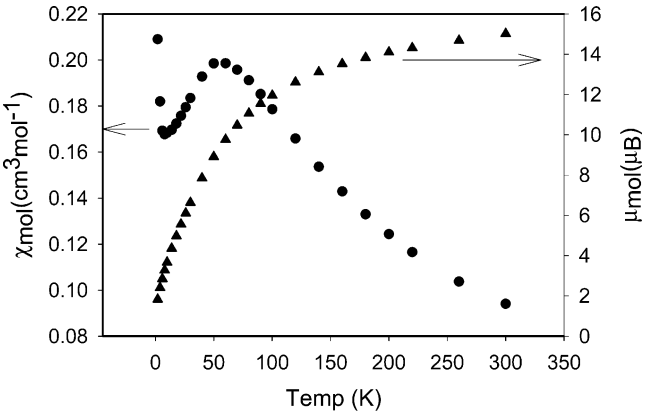

Figure 12. Magnetic profiles for **3** (χ_{mol}/T, μ_{mol}/T).

be expected. Clearly, J1 and J2 (Figure 6) must have comparable magnitudes in these cases.

Compound **9** has a magnetic profile identical to **7**,[14] indicating unoxidized manganese centers. Both **10** and **11** have magnetic profiles, which are essentially identical to **4** and **8**, indicating that on average only three electrons have been removed from the grid, leading to $S = {}^2/_2$ ground states. For **11**, this raises an important question concerning the situation where crystallographic structural results form the basis for the rationalization of other physical properties (vide supra). The average corner Mn bond distances in the structure of **11** clearly suggest that all four metal ions have been oxidized, but the bulk magnetic properties suggest that this is not the case, and only three electrons have been removed overall. This compound must be a mixture, with several oxidized grid components, and the structure was that of just one component in the crystalline sample.

The overall magnetic properties of the mixed oxidation state grid species are consistent with the electrochemical properties, which indicate that four electrons can be removed readily at potentials <1.0 V (vs Ag/AgCl) in an almost concerted process from four remote, and essentially equivalent, corner metal sites. Using a chemical approach, there is structural evidence for four-electron oxidation, but bulk magnetic properties indicate that a mixture of oxidized species is produced averaging to $[Mn(III)_3Mn(II)_6]$. It is easier to control the oxidation process electrochemically, and both structural evidence and magnetic evidence are consistent with a $[Mn(III)_4Mn(II)_5]$ species for **3**.

Conclusion

Grid platforms of redox active metal ions in close proximity, with bridging connections between all metal centers, provide a unique opportunity to examine cooperative properties within the grid. Electrochemical properties of a series of $[Mn(II)_9]$ grids have revealed that the more remote corner (α) sites do not communicate significantly, and all oxidize to Mn(III) at approximately the same potential. The side (*β*) centers feel the presence of neighboring sites through a combination of intramolecular electronic communication, and electrostatic Coulombic forces, and as a consequence the change in electronic properties of one oxidized site is communicated to a related site, with the result that metals

at these sites oxidize in a sequence of successively higher potentials. The molecular changes accompanying removal of the first four electrons from the corner sites are accompanied by the appearance of intense absorptions in the visible and near-infrared regions, associated with intervalence, Mn(II) ↔ Mn(III) charge transfer, and ligand-to-metal charge transfer, with corresponding changes in magnetic properties.

The ability to selectively remove four electrons from the $Mn(II)_9$ grids in a reversible and largely concerted process, with concomitant changes in both magnetic and optical properties, augers well for the use of such substrates in information storage and switching at the molecular level. The control over metal ion site oxidation state within a grid motif presents an exciting model system to test the encoding concept based on "quantum dot cellular automata" (QCA), in which the molecules are envisaged as structured charge containers, which can exist in degenerate states as a result of internal electron redistribution. Combinations of such subunits in close proximity, with appropriate electrostatic communication, could lead to "1" and "0" states.[43,44] In this context, it is of interest that self-assembled monolayers of such grids are easy to prepare on, e.g., gold surfaces,[17,45] with intergrid separations of <3 nm. Efforts are underway to exploit these properties and address individual molecules in surface monolayers.[17]

Acknowledgment. We thank the Natural Sciences and Engineering Research Council of Canada (NSERC) (L.K.T.), The Research Council of Norway (H.G.) (Postdoctoral Fellowship), and EPSRC (J.A.K.H.) (Senior Research Fellowship) for financial support for this study. Dr. R. McDonald (University of Alberta) is acknowledged for structural data on compound **1**, and D.O. Miller (Memorial University) for assistance with the structural solution of compound **1**. We also thank an astute reviewer for helpful comments concerning the comproportionation constant data.

Supporting Information Available: Magnetic (*M*/*H*) plot for **3** (Figure S1), and crystallographic data for **9**, **11** (Table S1). X-ray crystallographic data in CIF format for **1**, **3**, **9**−**11**. This material is available free of charge via the Internet at http://pubs.acs.org. Crystallographic data have also been deposited with the Cambridge Crystallographic Data Center, CCDC Nos. 249120−249124. Copies of this information may be obtained free of charge from The Director, CCDC, 12, Union Road, Cambridge, CB2 1EZ, U.K. (Fax: +44-1223-336033. E-mail: deposit@ccdc.cam. ac.uk.).

IC040083A

(43) Ruben, M.; Rojo, J.; Romero-Salguero, F. J.; Uppadine, L. H.; Lehn, J.-M. *Angew. Chem., Int. Ed.* **2004**, *43*, 3644.
(44) Lent, C. S.; Isaksen, B.; Lieberman, M. *J. Am. Chem. Soc.* **2003**, *125*, 1056.
(45) Weeks, L.; Thompson, L. K.; Shapter, J. G.; Pope, K. J.; Xu, Z. *J. Microscopy* **2003**, *212*, 102.